International Journal of Bifurcation and Chaos, Vol. 15, No. 7 (2005) 2207–2226

THE PISTON — CONNECTING ROD — CRANKSHAFT SYSTEM AS A TRIPLE PHYSICAL PENDULUM WITH IMPACTS

JAN AWREJCEWICZ and GRZEGORZ KUDRA
Technical University of Łódź,
Department of Automatics and Biomechanics (K–16)
1/15 Stefanowskiego St., 90-924 Łódź, Poland

Received November 5, 2003; Revised May 18, 2004

The triple physical pendulum with barriers is used to model a piston — connecting rod — crankshaft system of a mono-cylinder combustion engine. Among other results, a peculiar motion of the piston — connecting rod — crankshaft model is reported, i.e. six sliding stages of the piston along the cylinder per one engine cycle are illustrated. In spite of its simplicity, the introduced model can serve as the first step in a more advanced modeling taking into account various technological details. In particular, the proposed model can be considerably useful for the investigations of impacts between the piston and the cylinder aiming at the reduction or total elimination of this source of harmful noise.

Keywords: Triple pendulum; multibody; unilateral constraints; impact; piston dynamics.

1. Introduction

As known, even a single harmonically or parametrically excited pendulum may exhibit a rich spectrum of nonlinear phenomena including various local and global bifurcations, attractors and repellers, stable and unstable manifolds, scenarios leading to chaos and out of chaos, symmetry breaking and crisis bifurcations, steady-state and transitional chaos, oscillatory-rotational attractors, etc. (see [Bishop & Clifford, 1996; Szemplińska-Stupnicka & Tyrkiel, 2002a, 2002b; Szemplińska-Stupnicka *et al.*, 2000]).

On the other hand, many real processes, like for instance, earth-quake caused vibrations of high buildings can be modeled via coupled pendulums. It is clear that a couple system of pendulums may exhibit more complex nonlinear dynamics, and hence attracts the attention of mathematicians, physicists and engineers, who show a particular interest in the examination or control of various systems modeled by coupled pendulums. In addition, it may be expected that many theoretical unsolved problems of nonlinear dynamics can be explained using a model of rigid multibody coupled pendulums.

Our research is focused mainly on the application of triple pendulum dynamics to a real world object. It turns out that although many technological and design-oriented details have been neglected, the inverted triple pendulum can be used to model a real piston — connecting rod — crankshaft system of a mono-cylinder combustion engine.

Modeling of multibody systems with activity state of constraints varying during dynamics is addressed in references [Ballard, 2000; Pfeiffer, 1999; Wösle & Pfeiffer, 1999]. On the other hand, the problem of rigid impacts in multibody systems is illustrated and discussed in the monograph [Brogliato, 1999].

This paper is organized in the following manner. In Sec. 2, the general mathematical model of rigid multibody mechanical system with unilateral frictionless constraints is presented. Section 3

describes the generalized impact law used for impact modeling. In Sec. 4, the part of the model dealing with the sliding states is shown. The numerical algorithm for calculation of the system response is presented in Sec. 5. Section 6 contains the description of the general model of the triple physical pendulum with arbitrarily situated rigid and frictionless barriers. In Sec. 7, the piston — connecting rod — crankshaft system is modeled as a special case of the triple physical pendulum with barriers, and in Sec. 8 the numerical results devoted to its study are presented. Section 9 summarizes the research and presents the concluding remarks.

2. The Model of Rigid Multibody Mechanical System with Unilateral Frictionless Constraints

The concept of modeling of the rigid multibody mechanical system with unilateral constraints, when the activity state of a particular constraint may change during the system evolution, used in the present study, follows [Ballard, 2000; Pfeiffer, 1999; Wösle & Pfeiffer, 1999].

Let us consider a Lagrange rigid multibody mechanical system of n-degrees-of-freedom represented by the vector of generalized coordinates $\mathbf{q}(t) = [q_1(t), \ldots, q_n(t)]^T$ and subjected to the m unilateral constraints representing rigid frictionless obstacles imposed on the system position. If none of the unilateral constraints is active, the system dynamics is governed by the following set of the second-order differential equations:

$$\mathbf{M}(\mathbf{q}, t)\ddot{\mathbf{q}}(t) = \mathbf{f}(\mathbf{q}, \dot{\mathbf{q}}, t), \tag{1}$$

where $\mathbf{M}(\mathbf{q}, t)$ is the symmetric $n \times n$ inertia matrix, $\mathbf{f}(\mathbf{q}, \ddot{\mathbf{q}}, t)$ is the $n \times 1$ vector containing gyroscopic, damping, potential and exciting forces, $\dot{\mathbf{q}}(t)$ and $\ddot{\mathbf{q}}(t)$ are the $n \times 1$ vectors of generalized velocities and accelerations, respectively, and t is the independent time variable.

The rigid unilateral constraints are defined by the following set of algebraic inequalities:

$$\mathbf{h}(\mathbf{q}, t) \geq \mathbf{0}, \tag{2}$$

where $\mathbf{h}(\mathbf{q}, t) = [h_1(\mathbf{q}, t), \ldots, h_m(\mathbf{q}, t)]$ is the vector of m smooth scalar functions, and each of them should have a direct physical sense of the normal distance from the appropriate physical obstacle.

In order to describe the state of each potential constraint, the following index sets are introduced:

$$\begin{aligned} I &= \{1, 2, \ldots, m\}, \\ I_I &= \{i \in I; (h_i = 0 \wedge \dot{h}_i < 0)\}, \\ I_S &= \{i \in I; (h_i = 0 \wedge \dot{h}_i = 0 \wedge \lambda_i \geq 0)\}. \end{aligned} \tag{3}$$

The set I consists of m indexes of all potentially active constraints. The elements of the set I_I are represented by m_I indexes of the unilateral constraints with vanishing normal distance and negative relative velocity in the normal direction (the system is just before an impact with respect to these constraints). In the set I_S there are m_S indexes of the constraints with vanishing normal distance and vanishing relative velocity in the normal direction. The system is in the state of sliding on these obstacles acting on the system via non-negative normal reactions represented by non-negative Lagrange multipliers λ_i $(i \in I_S)$ that assure a continuous contact between bodies and the active obstacles $(\ddot{h}_i = 0,\ i \in I_S)$. The Lagrange multiplier λ_i represents a generalized normal force acting along the generalized coordinate h_i, where h_i is a real physical distance from the ith obstacle.

3. Generalized Impact Law

Since the investigated system is a Lagrangian one, it can be represented by a point moving in its configuration space $\mathbf{q}$ (see [Brogliato, 1999] for more details). The unilateral constraints define domains of this space, and the point representing the system strikes the boundaries of these domains. At the time instants $t = t_k$ of these "generalized" collisions, the system velocities undergo jumps, i.e. the vector of generalized velocities just before an impact $\dot{\mathbf{q}}(t_k^-) = \dot{\mathbf{q}}^-$ is transformed to the vector $\dot{\mathbf{q}}(t_k^+) = \dot{\mathbf{q}}^+$.

The presented model of impacts is the single impact model, i.e. we assume that the point representing configuration of the system strikes only one of the smooth surfaces $h_i(\mathbf{q}, t) = 0$ (the case of impact at the point on the curve of intersection of two surfaces, or impact with one, but nonsmooth surface is excluded). But we do not exclude the possibility of multiple impacts in the sense of finite number of single impacts, with not arbitrary, in general, succession, due to the algorithm presented in Sec. 5 and Fig. 1.

Now the method of calculating the post-impact velocities for a system with many degrees-of-freedom in the case of a single impact will be

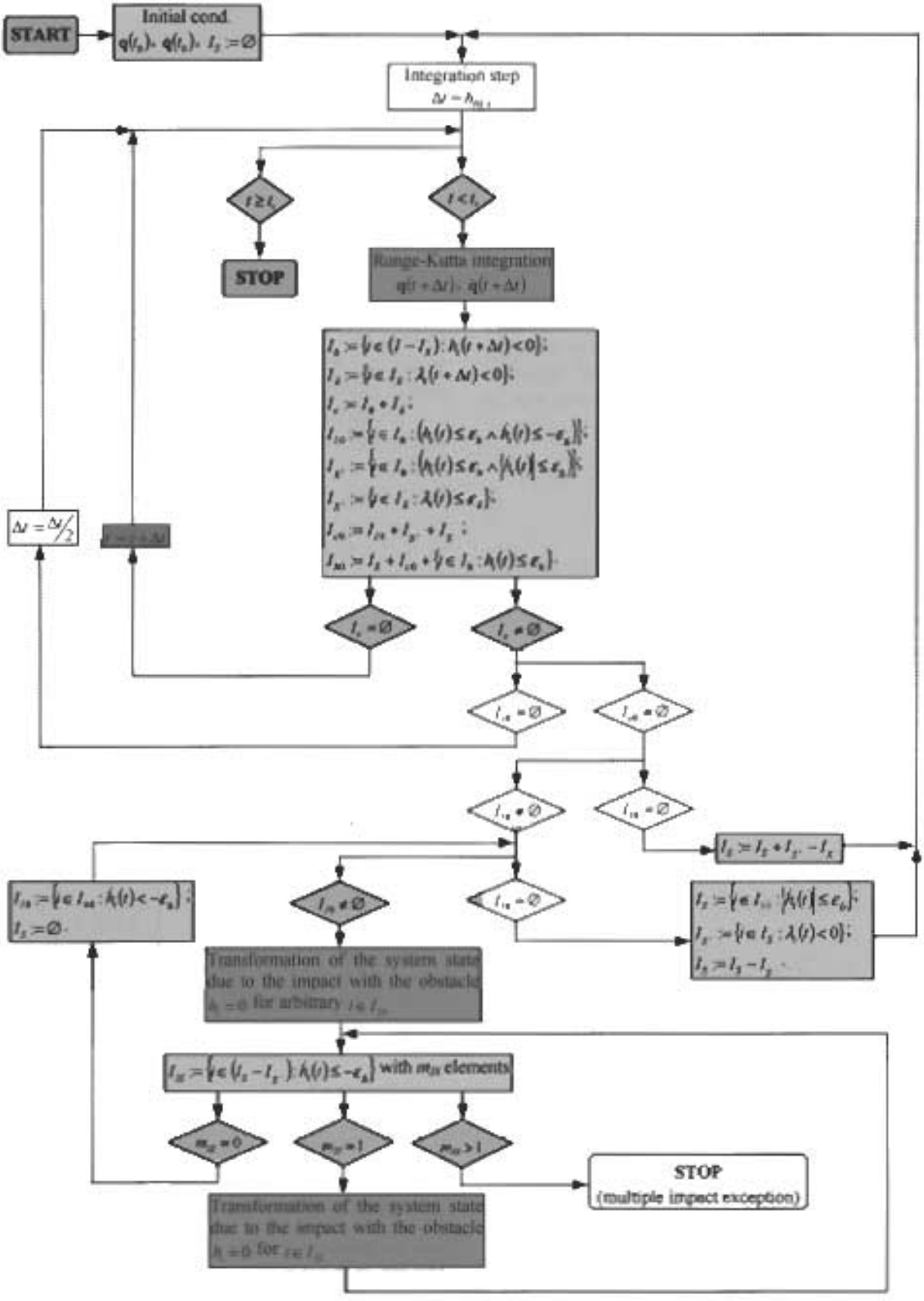

Fig. 1 Scheme of numerical simulation

outlined briefly in accordance with the description given in [Brogliato, 1999].

During an impact, the following shock dynamics equation is valid:

$$\mathbf{M}(\mathbf{q},t)\left(\dot{\mathbf{q}}^{+}-\dot{\mathbf{q}}^{-}\right)=\mathbf{p}_{\mathbf{q}}, \tag{4}$$

where $\mathbf{p}_{\mathbf{q}}$ is the generalized percussion vector for coordinates $\mathbf{q}$ (the force impulse vector generated by the impact).

For frictionless constraints, $\mathbf{p}_{\mathbf{q}}$ occurs along $\nabla_{\mathbf{q}}h_i(\mathbf{q},t)$ (because the interaction force due to the impact occurs along a Euclidean normal to the surface $h_i(\mathbf{q},t)=0$, which is yielded by the virtual work principle). Now, from (4) the following $n-1$ algebraic equations versus n unknowns can be obtained:

$$\mathbf{t}_{\mathbf{q},i,j}^{T}\,\mathbf{M}(\mathbf{q},t)\left(\dot{\mathbf{q}}^{+}-\dot{\mathbf{q}}^{-}\right)=0,\quad j=1,\ldots,n-1. \tag{5}$$

In the above, $\mathbf{t}_{\mathbf{q},i,j}$ are vectors tangent to the surface $h_i(\mathbf{q},t)=0$, chosen to be mutually independent, i.e. $\mathbf{t}_{\mathbf{q},i,j}^{T}\nabla_{\mathbf{q}}h_i(\mathbf{q},t)=0$ $(j=1,\ldots,n-1)$ and $\mathbf{t}_{\mathbf{q},i,j}^{T}\mathbf{t}_{\mathbf{q},i,k}=0$ $(j,k=1,\ldots,n-1)$.

The last lacking equation represents the extended Newton (restitution coefficient) rule applied to the relative velocity in the normal direction to the constraint

$$\dot{h}_i^{+}=-e_i\,\dot{h}_i^{-}, \tag{6}$$

where e_i is the restitution coefficient attached to the ith obstacle.

From (6) we obtain

$$\frac{\partial h_i}{\partial \mathbf{q}^{T}}\dot{\mathbf{q}}^{+}+\frac{\partial h_i}{\partial t}=-e_i\left(\frac{\partial h_i}{\partial \mathbf{q}^{T}}\dot{\mathbf{q}}^{-}+\frac{\partial h_i}{\partial t}\right). \tag{7}$$

Owing to (5), it is seen that there is (in general) a discontinuity in the tangential velocity due to the inertia coupling.

A change of the kinetic energy at impact is defined by the formula

$$\Delta T(t_k)=\frac{1}{2}\left(\dot{\mathbf{q}}^{+}\right)^{T}\mathbf{M}(\mathbf{q},t)\dot{\mathbf{q}}^{+}-\frac{1}{2}\left(\dot{\mathbf{q}}^{-}\right)^{T}\mathbf{M}(\mathbf{q},t)\dot{\mathbf{q}}^{-}. \tag{8}$$

From (8), using (5) and (7) and on the account of the assumption that the constraint is stationary $(\partial h_i/\partial t=0)$, one arrives at

$$\Delta T\left(t_k\right)=\frac{1}{2}\left(e_i^{2}-1\right)\cdot\left(\frac{\mathbf{M}(\mathbf{q},t)^{-1}\nabla_{\mathbf{q}}h_i}{\sqrt{\left(\nabla_{\mathbf{q}}h_i\right)^{T}\mathbf{M}(\mathbf{q},t)^{-1}\nabla_{\mathbf{q}}h_i}}\mathbf{M}(\mathbf{q},t)\dot{\mathbf{q}}^{-}\right)^{2}. \tag{9}$$

Observe that for $0\le e_i\le 1$, the kinetic energy change due to impact is $\Delta T(t_k)\le 0$, for $e_i=1$, it is $\Delta T(t_k)=0$, and for $e_i=0$, $\Delta T(t_k)$ reaches its lowest possible value.

To summarize, when the system achieves a discontinuity point at the time instant $t=t_k$ indicated by $h_i(\mathbf{q}(t_k),t_k)=0$, the vector of velocities is transformed via the relation

$$\dot{\mathbf{q}}\left(t_k^{+}\right)=\mathbf{g}_i\left(\mathbf{q}(t_k),\dot{\mathbf{q}}(t_k^{-}),t_k\right), \tag{10}$$

where the vector function $\mathbf{g}_i(\mathbf{q},\dot{\mathbf{q}},t)$ is derived from (5) and (7), and has the following form

$$\mathbf{g}_i(\mathbf{q},\dot{\mathbf{q}},t)=\left[\begin{array}{c}\left(\nabla_{\mathbf{q}}h_i(\mathbf{q},t)\right)^{T}\\ \left[\begin{array}{c}\mathbf{t}_{\mathbf{q},i,1}^{T}\\ \cdots\\ \mathbf{t}_{\mathbf{q},i,n-1}^{T}\end{array}\right]\cdot\mathbf{M}(\mathbf{q},t)\end{array}\right]^{-1}\cdot\left(\left[\begin{array}{c}-e_i\left(\nabla_{\mathbf{q}}h_i(\mathbf{q},t)\right)^{T}\\ \left[\begin{array}{c}\mathbf{t}_{\mathbf{q},i,1}^{T}\\ \cdots\\ \mathbf{t}_{\mathbf{q},i,n-1}^{T}\end{array}\right]\cdot\mathbf{M}(\mathbf{q},t)\end{array}\right]\dot{\mathbf{q}}+\left\{\begin{array}{c}-\left(e_i+1\right)\dfrac{\partial h_i(\mathbf{q},t)}{\partial t}\\ 0\\ \cdots\\ 0\end{array}\right\}\right). \tag{11}$$

4. Sliding States along Some Obstacles

Let us assume that the set I_I is empty $(m_I=0)$ and the set of indexes of continuously active constraints has the following form:

$$I_S=\{i_1,i_2,\ldots,i_{m_S}\}. \tag{12}$$

In what follows, the $m_S \times 1$ vector corresponding to notation (12) is defined as

$$\mathbf{h}_S(\mathbf{q},t) = \left\{ \begin{array}{c} h_{i_1}(\mathbf{q},t) \\ h_{i_2}(\mathbf{q},t) \\ \cdots \\ h_{i_{m_S}}(\mathbf{q},t) \end{array} \right\}, \tag{13}$$

containing all functions $h_i(\mathbf{q},t)$ that represent continuously active obstacles.

The vector of Lagrange multipliers

$$\boldsymbol{\lambda}_S = \left\{ \begin{array}{c} \lambda_{i_1} \\ \lambda_{i_2} \\ \cdots \\ \lambda_{i_{m_S}} \end{array} \right\} \tag{14}$$

is attached to vector (13), where $\lambda_{i_k} \geq 0$ for $k = 1,2,\ldots,m_S$.

In order to describe the system dynamics, normal reactions generated by active constraints acting on the system are introduced to Eq. (1) via Lagrange multipliers

$$\mathbf{M}\ddot{\mathbf{q}} = \mathbf{f} + \left(\frac{\partial \mathbf{h}_S}{\partial \mathbf{q}^T}\right)^T \boldsymbol{\lambda}_S. \tag{15}$$

The continuous contact between the active constraint surfaces and the bodies of the system implies the following condition:

$$\ddot{\mathbf{h}}_S = \frac{\partial \mathbf{h}_S}{\partial \mathbf{q}^T}\ddot{\mathbf{q}} + \dot{\mathbf{q}}^T \frac{\partial^2 \mathbf{h}_S}{\partial \mathbf{q}\partial \mathbf{q}^T}\dot{\mathbf{q}} + 2\frac{\partial^2 \mathbf{h}_S}{\partial t \partial \mathbf{q}^T}\dot{\mathbf{q}} + \frac{\partial^2 \mathbf{h}_S}{\partial t^2} = 0. \tag{16}$$

Equations (15) and (16) create the following set of differential-algebraic equations governing the system [Strzałko & Grabski, 1997]

$$\begin{bmatrix} \mathbf{M} & \mathbf{A}^T \\ \mathbf{A} & \mathbf{0} \end{bmatrix} \left\{ \begin{array}{c} \ddot{\mathbf{q}} \\ \boldsymbol{\lambda}_S \end{array} \right\} = \left\{ \begin{array}{c} \mathbf{f} \\ \mathbf{d} \end{array} \right\}, \tag{17}$$

where

$$\mathbf{A} = -\frac{\partial \mathbf{h}_S}{\partial \mathbf{q}^T}, \qquad \mathbf{d} = \dot{\mathbf{q}}^T \frac{\partial^2 \mathbf{h}_S}{\partial \mathbf{q}\partial \mathbf{q}^T}\dot{\mathbf{q}} + 2\frac{\partial^2 \mathbf{h}_S}{\partial t \partial \mathbf{q}^T}\dot{\mathbf{q}} + \frac{\partial^2 \mathbf{h}_S}{\partial t^2}. \tag{18}$$

Introducing the vector

$$\mathbf{U} = \begin{bmatrix} \mathbf{U}_{11} & \mathbf{U}_{12} \\ \mathbf{U}_{21} & \mathbf{U}_{22} \end{bmatrix} = \begin{bmatrix} \mathbf{M} & \mathbf{A}^T \\ \mathbf{A} & \mathbf{0} \end{bmatrix}^{-1}, \tag{19}$$

the following set of differential-algebraic equations is obtained

$$\begin{aligned} \ddot{\mathbf{q}} &= \mathbf{U}_{11}\,\mathbf{f} + \mathbf{U}_{12}\,\mathbf{d}, \\ \boldsymbol{\lambda}_S &= \mathbf{U}_{21}\,\mathbf{f} + \mathbf{U}_{22}\,\mathbf{d}. \end{aligned} \tag{20}$$

5. Computational Model

A numerical scheme for calculation of the system response is presented in Fig. 1. The scheme applies the Runge–Kutta method of fourth order with a nominal time step h_{RK4} in time intervals (t_j, t_{j+1}), where the set I_I is empty (there is no impact) and the set I_S does not change. The discontinuity points t_j and t_{j+1} are detected with a finite precision by halving the integration step. At those points, appropriate changes of the set I_S members are introduced as well as possible transformations of the velocity vector generated by the impact. The symbols ε_h, $\varepsilon_{\dot{h}}$ and ε_λ denote the obstacle detection accuracy, the detection accuracy of the zero of the normal component of the relative velocity, and the detection accuracy of the zero of the normal force with respect to the barrier surface, respectively.

Notice, that the multiple impacts [Ballard, 2000; Brogliato, 1999] are now possible, a series of a finite number of single impacts, with succession determined by the algorithm presented in Fig. 1. In most cases this succession is strictly determined. This is the case when the initial conditions before each single impact are such that the system "tries" to penetrate the space not allowed by only one algebraic condition. But sometimes the situation is possible, when the system "tries" to violate more than one unilateral constraint $h_i \geq 0$ simultaneously. In such situations our algorithm recognizes two cases: the first one, when it is possible to assume the first single impact with one constraint, chosen arbitrarily from considered ones ($h_i = 0$, $i \in I_{I0}$), and the second case, when it is not possible ($h_i = 0$, $i \in I_{IS}$, the case not encountered in our simulation examples). The example of the first case is the situation, when the trajectory, initially without contact with constraints 1 and 2, pierces at some time instance two surfaces 1 and 2 simultaneously, i.e. it crosses the curve of intersection of these two surfaces, and "tries" to penetrate, after that time instance, the space not allowed by the two algebraic conditions. But such a case is not generic and the probability of its appearance is infinitely small. On the other hand, in our numerical simulations, the

precision of the computed trajectory is finite and the determination of impact point has also finite precision and such a case is possible in our algorithm. But, in this case, we can choose one of these two constraints for the first single impact arbitrarily, since it is contained in the tolerance of simulation. The example of the second case is the situation, when the trajectory initially lying on the curve of intersection of two surfaces 1 and 2, at some time instance, impacts the third surface 3. Firstly the single impact against the surface 3 takes place. Let us assume, that after this impact, the new initial conditions are such that the system tries to penetrate both barriers 1 and 2. It is a generic case and the impact is strictly with two surfaces simultaneously. In such a case, the simulation stops and returns the "multiple impact exception" message.

6. Triple Physical Pendulum with Barriers

A sketch of the general model of the triple physical pendulum moving in the plane of a global co-ordinate system $\overline{x}, \overline{y}$ (with origin at point O_1) and being a special case of the model introduced in the previous sections is presented in Fig. 2. It is assumed that the links are absolute stiff bodies moving in a vacuum and coupled by viscous damping with coefficients $\vec{r}_i$ $(i = 1, 2, 3)$. Each of the links can be externally forced by $\overline{f}_{e,i}$ $(i = 1, 2, 3)$. It is also assumed that (i) the mass centers of the links lie on the lines including joints O_i; (ii) one of the principal central inertia axes of each link (z_{C_i}) is perpendicular to a movement plane $\overline{x} - \overline{y}$. The position of the system is described by three angles ψ_i $(i = 1, 2, 3)$.

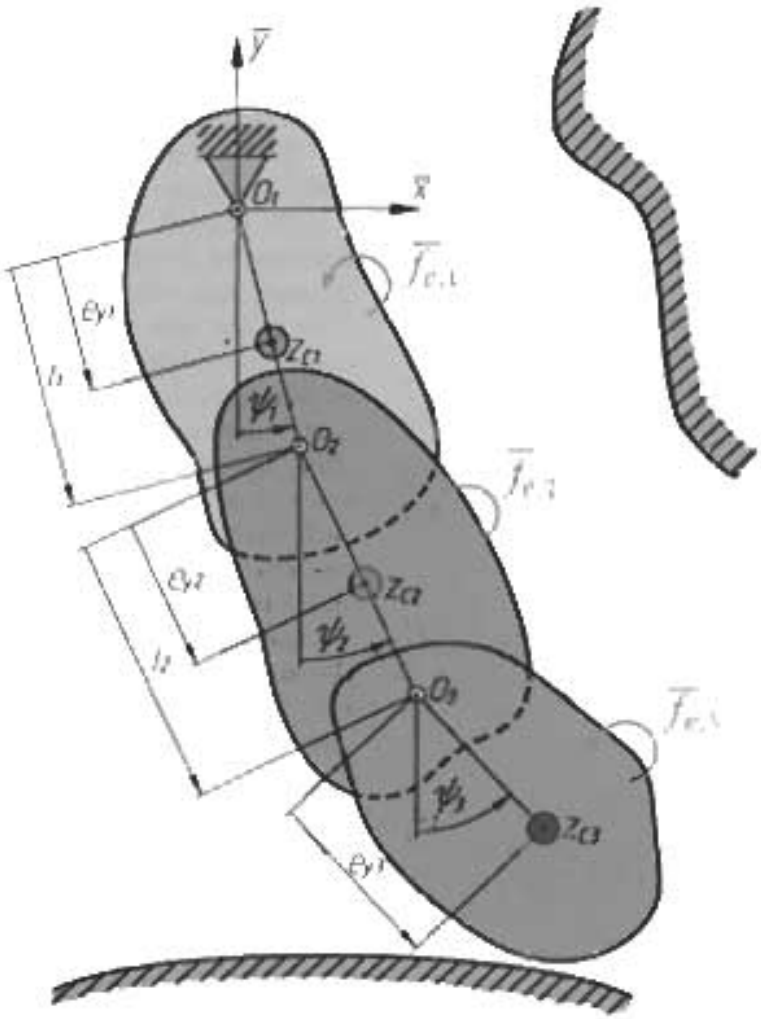

Fig. 2. Triple physical pendulum with obstacles

On the position of the system, the set of arbitrarily situated rigid and frictionless barriers can be imposed. The system is governed by a nondimensional set of ordinary differential equations without obstacles plus a set of algebraic inequalities (unilateral constraints) representing barriers with the corresponding restitution coefficients (e_i) of the form:

$$\mathbf{M}(\boldsymbol{\psi})\,\ddot{\boldsymbol{\psi}} + \mathbf{N}(\boldsymbol{\psi})\,\dot{\boldsymbol{\psi}}^{\mathbf{2}} + \boldsymbol{C}\,\dot{\boldsymbol{\psi}} + \mathbf{p}(\boldsymbol{\psi}) = \mathbf{f}_e(\boldsymbol{\psi}, \dot{\boldsymbol{\psi}}, t), \tag{21a}$$

$$h_i(\boldsymbol{\psi}) \geq 0, \quad i = 1, \ldots, m \tag{21b}$$

where

$$\boldsymbol{\psi} = \begin{Bmatrix} \psi_1 \\ \psi_2 \\ \psi_3 \end{Bmatrix}, \quad \ddot{\boldsymbol{\psi}} = \begin{Bmatrix} \ddot{\psi}_1 \\ \ddot{\psi}_2 \\ \ddot{\psi}_3 \end{Bmatrix}, \quad \dot{\boldsymbol{\psi}}^{\mathbf{2}} = \begin{Bmatrix} \dot{\psi}_1^2 \\ \dot{\psi}_2^2 \\ \dot{\psi}_3^2 \end{Bmatrix}, \quad \dot{\boldsymbol{\psi}} = \begin{Bmatrix} \dot{\psi}_1 \\ \dot{\psi}_2 \\ \dot{\psi}_3 \end{Bmatrix}, \tag{22a}$$

$$\mathbf{M}(\boldsymbol{\psi}) = \begin{bmatrix} 1 & \nu_{12}\cos(\psi_1 - \psi_2) & \nu_{13}\cos(\psi_1 - \psi_3) \\ \nu_{12}\cos(\psi_1 - \psi_2) & \beta_2 & \nu_{23}\cos(\psi_2 - \psi_3) \\ \nu_{13}\cos(\psi_1 - \psi_3) & \nu_{23}\cos(\psi_2 - \psi_3) & \beta_3 \end{bmatrix},$$

$$\mathbf{N}(\boldsymbol{\psi}) = \begin{bmatrix} 0 & \nu_{12}\sin(\psi_1 - \psi_2) & \nu_{13}\sin(\psi_1 - \psi_3) \\ -\nu_{12}\sin(\psi_1 - \psi_2) & 0 & \nu_{23}\sin(\psi_2 - \psi_3) \\ -\nu_{13}\sin(\psi_1 - \psi_3) & -\nu_{23}\sin(\psi_2 - \psi_3) & 0 \end{bmatrix}, \tag{22b}$$

$$\mathbf{C} = \begin{bmatrix} c_1 + c_2 & -c_2 & 0 \\ -c_2 & c_2 + c_3 & -c_3 \\ 0 & -c_3 & c_3 \end{bmatrix}, \quad \mathbf{p}(\boldsymbol{\psi}) = \begin{Bmatrix} \sin\psi_1 \\ \mu_2 \sin\psi_2 \\ \mu_3 \sin\psi_3 \end{Bmatrix}, \quad \mathbf{f}_e(\boldsymbol{\psi}, \dot{\boldsymbol{\psi}}, t) = \begin{Bmatrix} f_{e,1}(\boldsymbol{\psi}, \dot{\boldsymbol{\psi}}, t) \\ f_{e,2}(\boldsymbol{\psi}, \dot{\boldsymbol{\psi}}, t) \\ f_{e,3}(\boldsymbol{\psi}, \dot{\boldsymbol{\psi}}, t) \end{Bmatrix}.$$

The following relations hold between the nondimensional quantities and the physical ones .

$$t = \alpha_1 \tau,$$

$$\dot{\psi}_j = \alpha_1^{-1} \overset{\prime}{\psi}_j, \quad \ddot{\psi}_j = \alpha_1^{-2} \overset{\prime\prime}{\psi}_j, \quad j = 1, 2, 3 \tag{23a}$$

$$\alpha_1 = \left(M_1 B_1^{-1}\right)^{\frac{1}{2}}, \tag{23b}$$

$$\beta_2 = \frac{B_2}{B_1}, \quad \beta_3 = \frac{B_3}{B_1}$$

$$\nu_{12} = \frac{N_{12}}{B_1}, \quad \nu_{13} = \frac{N_{13}}{B_1}, \quad \nu_{23} = \frac{N_{23}}{B_1}, \tag{23c}$$

$$\mu_2 = \frac{M_2}{M_1}, \quad \mu_3 = \frac{M_3}{M_1},$$

$$c_j = \frac{\bar{c}_j}{\sqrt{M_1 B_1}}, \quad f_{e,j} = \frac{\bar{f}_{e,j}}{M_1}, \quad j = 1, 2, 3, \tag{23d}$$

where symbols $\overset{\prime}{(\ldots)}$ and $\dot{(\ldots)}$ denote derivatives with respect to real time t and nondimensional time τ, respectively, and where the following notation is used:

$$\begin{aligned} B_1 &= J_{z1} + e_{y1}^2 m_1 + l_1^2 (m_2 + m_3), \\ B_2 &= J_{z2} + e_{y2}^2 m_2 + l_2^2 m_3, \\ B_3 &= J_{z3} + e_{y3}^2 m_3, \\ N_{12} &= m_2 e_{y2} l_1 + m_3 l_1 l_2, \\ N_{13} &= m_3 e_{y3} l_1, \\ N_{23} &= m_3 e_{y3} l_2, \\ M_1 &= m_1 g e_{y1} + (m_2 + m_3)\, g l_1, \\ M_2 &= m_2 g e_{y2} + m_3 g l_2, \\ M_3 &= m_3 g e_{y3}. \end{aligned} \tag{24}$$

In the above, J_{zi} $(i = 1, 2, 3)$ denote appropriate principal central moments of inertia, m_i $(i = 1, 2, 3)$ denote masses of respective links and g is the gravitational acceleration.

The functions $h_i(\psi)$ represent distances of the system from an appropriate obstacle. More details of the triple physical pendulum model can be found in [Awrejcewicz *et al.*, 2001, 2002, 2003; Kudra, 2002].

7. Piston — Connecting Rod — Crankshaft System

The general model of the triple physical pendulum with barriers, introduced in Sec. 2, can be used to build a model of the piston — connecting rod — crankshaft system of the mono-cylinder combustion engine shown in Fig. 3. The first link represents the crankshaft (1), the second one is the connecting rod (2) and the third one is the piston (3). The links are connected by rotational joints with viscous damping. The cylinder barrel imposes restrictions on the position of the piston that moves in the cylinder with backlash. It is assumed that at the contact of the surfaces between the piston and the cylinder a tangent force does not appear. Observe that the model of the piston — connecting rod — crankshaft system can be treated as an inverted pendulum, so it is natural to introduce the following vector of angles describing the system position

$$\begin{aligned}\boldsymbol{\phi} &= [\varphi_1, \varphi_2, \varphi_3]^T \\ &= [\psi_1 + \pi, \psi_2 + \pi, \psi_3 + \pi]^T, \end{aligned} \tag{25}$$

where angles ψ_i $(i = 1, 2, 3)$ are the generalized co-ordinates used in Sec. 2 for the description of the general triple physical pendulum.

The restriction on the position of the piston imposed by the cylinder barrel can be described using four conditions defined by four points K_i $(i = 1, 2, 3, 4)$:

$$\begin{aligned}
\overline{x}_{K_1} &= -l_1 \sin\varphi_1 - l_2 \sin\varphi_2 - h \sin\varphi_3 \\
&\quad - \frac{d}{2}\cos\varphi_3 \geq -\frac{D}{2}, \\
\overline{x}_{K_2} &= -l_1 \sin\varphi_1 - l_2 \sin\varphi_2 - h \sin\varphi_3 \\
&\quad - \frac{d}{2}\cos\varphi_3 + s \sin\varphi_3 \geq -\frac{D}{2}, \\
\overline{x}_{K_3} &= -l_1 \sin\varphi_1 - l_2 \sin\varphi_2 - h \sin\varphi_3 \\
&\quad + \frac{d}{2}\cos\varphi_3 \leq \frac{D}{2}, \\
\overline{x}_{K_4} &= -l_1 \sin\varphi_1 - l_2 \sin\varphi_2 - h \sin\varphi_3 \\
&\quad + \frac{d}{2}\cos\varphi_3 + s \sin\varphi_3 \leq \frac{D}{2},
\end{aligned} \tag{26}$$

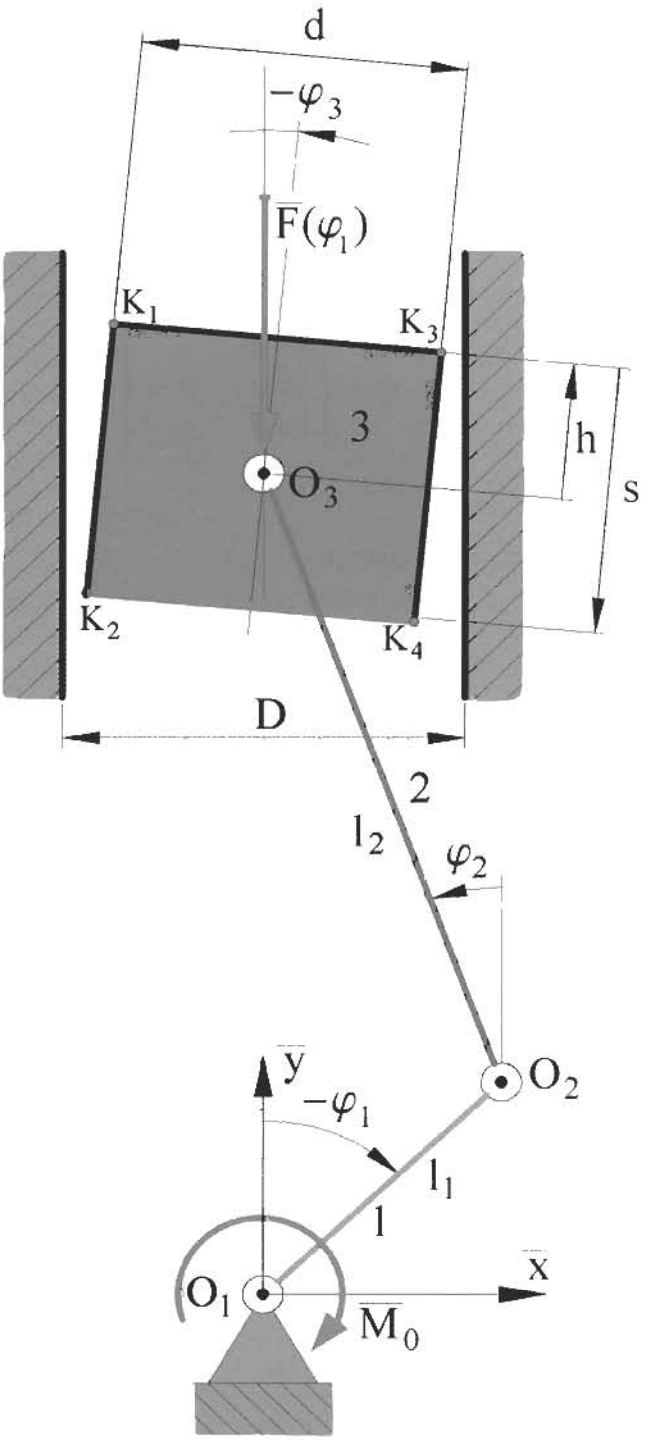

Fig. 3. Piston — connecting rod — crankshaft system.

where $\overline{x}_{K_1}$, $\overline{x}_{K_2}$, $\overline{x}_{K_3}$ and $\overline{x}_{K_4}$ are co-ordinates of four corners of the piston in the co-ordinate system $\overline{x} - \overline{y}$. Notice that the given description is valid only when the piston does not undergo full rotation (i.e. the backlash is sufficiently small).

The above inequalities are divided by l_1 and transformed to the form

$$h_1(\phi) = \frac{\overline{x}_{K_1} + \frac{D}{2}}{l_1} \geq 0, \quad h_2(\phi) = \frac{\overline{x}_{K_2} + \frac{D}{2}}{l_1} \geq 0,$$
$$h_3(\phi) = \frac{-\overline{x}_{K_3} + \frac{D}{2}}{l_1} \geq 0, \quad h_4(\phi) = \frac{-\overline{x}_{K_4} + \frac{D}{2}}{l_1} \geq 0, \tag{27}$$

yielding the final form of the nondimensional set of inequalities (representing rigid unilateral constraints):

$$\begin{aligned} h_1(\phi) &= \frac{\Delta}{2} - \sin\varphi_1 - \lambda_2 \sin\varphi_2 \\ &\quad - \eta \sin\varphi_3 - \frac{\delta}{2}\cos\varphi_3 \geq 0, \\ h_2(\phi) &= \frac{\Delta}{2} - \sin\varphi_1 - \lambda_2 \sin\varphi_2 \\ &\quad + (\sigma - \eta)\sin\varphi_3 - \frac{\delta}{2}\cos\varphi_3 \geq 0, \\ h_3(\phi) &= \frac{\Delta}{2} + \sin\varphi_1 + \lambda_2 \sin\varphi_2 \\ &\quad + \eta \sin\varphi_3 - \frac{\delta}{2}\cos\varphi_3 \geq 0, \\ h_4(\phi) &= \frac{\Delta}{2} + \sin\varphi_1 + \lambda_2 \sin\varphi_2 \\ &\quad - (\sigma - \eta)\sin\varphi_3 - \frac{\delta}{2}\cos\varphi_3 \geq 0, \end{aligned} \tag{28}$$

where the following nondimensional parameters are introduced

$$\lambda_2 = \frac{l_2}{l_1}, \quad \eta = \frac{h}{l_1}, \quad \sigma = \frac{s}{l_1}, \quad \delta = \frac{d}{l_1}, \quad \Delta = \frac{D}{l_1}. \tag{29}$$

The same restitution coefficient e is related to each of the unilateral constraints.

It is assumed that a gas pressure force can be reduced to the force acting along a line parallel to the axis of the cylinder and containing the piston pin axis O_3. Moreover, this force is assumed to be a function of the angular position of the crankshaft φ_1

$$\overline{F}(\varphi_1) = p_{\max} \frac{\pi d^2}{4} p(\varphi_1), \tag{30}$$

where $p_{\max}$ is the maximal pressure over the piston, and $p(\varphi_1)$ is the nondimensional pressure distribution such that its maximal value is one. The pressure distribution function with period $2\pi N$ (where N is an integer number) is developed into a Fourier series with a finite number of terms K

$$p(\varphi_1) = a_0 + \sum_{i=1}^{K} a_i \cos\left(i\frac{\varphi_1}{N}\right) + \sum_{i=1}^{K} b_i \sin\left(i\frac{\varphi_1}{N}\right). \tag{31}$$

The crankshaft is externally driven by moment $\overline{M}_0$ originating from an external power receiver (brake) and acting contrary to the positive sense of the angle φ_1. It is also assumed that the rotational speed of the crankshaft is constant. The system defined in such a way is in fact an autonomous and self-excited system.

The external forces acting on the system can be reduced to the following generalized force vector:

$$\overline{\mathbf{f}}_e(\phi) = \begin{Bmatrix} \overline{F}(\varphi_1)\, l_1 \sin\varphi_1 - \overline{M}_0 \\ \overline{F}(\varphi_1)\, l_2 \sin\varphi_2 \\ 0 \end{Bmatrix}, \tag{32}$$

where $\overline{f}_{e,1}$ is the moment of force acting on the crankshaft system, $\overline{f}_{e,2}$ is the moment acting on the connecting rod and $\overline{f}_{e,3}$ is equal to zero (the latter observation is yielded assuming that the gas pressure force acts along the line including point O_3).

The nondimensional equations of motion, when none of the obstacles is active, are as follows:

$$\mathbf{M}(\phi)\ddot{\phi} + \mathbf{N}(\phi)\dot{\phi}^2 + \mathbf{C}\dot{\phi} + \mathbf{p}(\phi) = \mathbf{f}_e(\phi), \tag{33}$$

where

$$\ddot{\phi} = \ddot{\psi}|_{\psi=\phi}, \quad \dot{\phi}^2 = \dot{\psi}^2|_{\psi=\phi}, \quad \dot{\phi} = \dot{\psi}|_{\psi=\phi},$$
$$\mathbf{M}(\phi) = \mathbf{M}(\psi)|_{\psi=\phi}, \quad \mathbf{N}(\phi) = \mathbf{N}(\psi)|_{\psi=\phi}, \tag{34}$$
$$\mathbf{p}(\phi) = -\mathbf{p}(\psi)|_{\psi=\phi},$$

In the above, the nondimensional generalized force vector takes the following explicit form:

$$\mathbf{f}_e(\phi) = \frac{\overline{\mathbf{f}}_e(\phi)}{M_1} = \begin{Bmatrix} F_0\, p(\varphi_1) \sin\varphi_1 - M_0 \\ \lambda_2\, F_0\, p\,(\varphi_1) \sin\varphi_2 \\ 0 \end{Bmatrix}, \tag{35}$$

where the following nondimensional parameters are introduced:

$$F_0 = p_{\max} \frac{\pi d^2}{4} \frac{l_1}{M_1}, \quad M_0 = \frac{\overline{M}_0}{M_1}. \tag{36}$$

Predicting large rotational speeds of the crankshaft, it is reasonable to introduce a new nondimensional time

$$t = \alpha_1 t, \tag{37}$$

where α_1 is the average nondimensional angular velocity (measured in the nondimensional time t) of the crankshaft per period (corresponding to the period $2\pi N$ of the pressure function $p(\varphi_1)$) of the periodic steady state motion of the system without backlash between the piston and the cylinder ($d = D$). The new nondimensional time is scaled in such a way that the corresponding nondimensional angular velocity of the shaft is approximately equal to one, which is more convenient for the simulations and analysis.

In this special case ($d = D$) the analyzed system reduces to a one-degree-of-freedom system, and the generalized co-ordinates vector has independent components

$$\boldsymbol{\phi} = \begin{Bmatrix} \varphi_1 \\ \varphi_2(\varphi_1) \\ 0 \end{Bmatrix}. \tag{38}$$

The geometric and kinematic relations between the co-ordinates of the given vector, and between their derivatives follow

$$\sin(\varphi_2) = -\lambda_2^{-1}\sin(\varphi_1),$$
$$\cos(\varphi_2) = \sqrt{1-\lambda_2^{-2}\sin^2\varphi_1},$$
$$\text{for } \lambda_2 > 1 \quad \text{and} \quad \varphi_2 \in \left(-\frac{\pi}{2}, \frac{\pi}{2}\right),$$
$$\frac{\partial\varphi_2}{\partial\varphi_1} = -\lambda_2^{-1}\frac{\cos\varphi_1}{\cos\varphi_2} = -\lambda_2^{-1}\frac{\cos\varphi_1}{\sqrt{1-\lambda_2^{-2}\sin^2\varphi_1}},$$
$$\dot{\varphi}_2 = \frac{\partial\varphi_2}{\partial\varphi_1}\dot{\varphi}_1 = -\lambda_2^{-1}\frac{\cos\varphi_1}{\sqrt{1-\lambda_2^{-2}\sin^2\varphi_1}}\dot{\varphi}_1, \tag{39}$$
$$d\varphi_2 = \frac{\partial\varphi_2}{\partial\varphi_1}d\varphi_1 = -\lambda_2^{-1}\frac{\cos\varphi_1}{\sqrt{1-\lambda_2^{-2}\sin^2\varphi_1}}d\varphi_1.$$

The average angular velocity is defined by the formula

$$L_d + L_e = 0, \tag{40}$$

where L_d and L_e denote correspondingly the viscous damping forces work and the external forces work during one period of the steady state motion of the system without backlash between the piston and the cylinder.

The viscous damping forces work can be written as

$$L_d = -\int_T (\mathbf{C}\dot{\boldsymbol{\phi}})\,d\boldsymbol{\phi}^T = -\int_0^{2\pi N} \left(\begin{bmatrix} c_1+c_2 & 0 \\ -c_2 & c_2+c_3 \\ 0 & -c_3 \end{bmatrix} \begin{Bmatrix} \dot{\varphi}_1 \\ \frac{\partial\varphi_2}{\partial\varphi_1}\dot{\varphi}_1 \\ 0 \end{Bmatrix} \right) \begin{Bmatrix} d\varphi_1 \\ \frac{\partial\varphi_2}{\partial\varphi_1}d\varphi_1 \\ 0 \end{Bmatrix}^T. \tag{41}$$

Using relations (39) and replacing the angular velocity $\dot{\varphi}_1$ by the average velocity α_1, relation (41) can be expressed as follows:

$$L_d = -(c_1+c_2)\alpha_1\int_0^{2\pi N} d\varphi_1 - 2\lambda_2^{-1}c_2\alpha_1\int_0^{2\pi N}\frac{\cos\varphi_1}{\sqrt{1-\lambda_2^{-2}\sin^2\varphi_1}}d\varphi_1 - \lambda_2^{-2}(c_2+c_3)\alpha_1\int_0^{2\pi N}\frac{\cos^2\varphi_1}{1-\lambda_2^{-2}\sin^2\varphi_1}d\varphi_1. \tag{42}$$

After integration, the following expression obtained for the damping forces work as a function of the average angular velocity:

$$L_d = -2\pi N((c_1+c_2) + \lambda_2^{-1}(c_2+c_3)(1-\sqrt{1-\lambda_2^{-2}}))\alpha_1. \tag{43}$$

The nonrestoring external forces can be cast in the form

$$L_e = \int_T \mathbf{f}_e(\boldsymbol{\phi})\,d\boldsymbol{\phi}^T = \int_0^{2\pi N} \begin{Bmatrix} F_0\,p(\varphi_1)\sin\varphi_1 - M_0 \\ \lambda_2 F_0\,p(\varphi_1)\sin\varphi_2 \\ 0 \end{Bmatrix} \begin{Bmatrix} d\varphi_1 \\ \frac{\partial\varphi_2}{\partial\varphi_1}d\varphi_1 \\ 0 \end{Bmatrix}^T. \tag{44}$$

From the given expression, and using (39) one gets

$$L_e = L_F + L_M, \tag{45}$$

where

$$L_F = F_0\int_0^{2\pi N} p(\varphi_1)\sin\varphi_1 \cdot\left(1+\frac{\cos\varphi_1}{\lambda_2\sqrt{1-\lambda_2^{-2}\sin^2\varphi_1}}\right)d\varphi_1,$$
$$L_M = -2\pi N M_0 \tag{46}$$

represent the work of the nondimensional gas pressure forces and the work of the nondimensional external moment loading the shaft, respectively.

Condition (40) and relations (43), (45) and (46) yield the following form of the average angular velocity of the shaft

$$\alpha_1 = F_0 \frac{\displaystyle\int_0^{2\pi N} p(\varphi_1)\sin\varphi_1\left(1+\frac{\cos\varphi_1}{\lambda_2\sqrt{1-\lambda_2^{-2}\sin^2\varphi_1}}\right)d\varphi_1 - 2\pi N M_0}{2\pi N((c_1+c_2)+\lambda_2^{-1}(c_2+c_3)(1-\sqrt{1-\lambda_2^{-2}}))}. \tag{47}$$

Let $(\overset{\circ}{\ldots})$ denote the derivative with respect to time $\not{t}$, whereas relations between derivatives with respect to nondimensional time t, real time τ and new nondimensional time $\not{t}$ have the form

$$\begin{aligned}\frac{d(\ldots)}{dt} &= \frac{d(\ldots)}{d\not{t}}\frac{d\not{t}(t)}{dt} = \alpha_1\frac{d(\ldots)}{d\not{t}},\\ \frac{d(\ldots)}{d\tau} &= \frac{d(\ldots)}{d\not{t}}\frac{d\not{t}(t)}{dt}\frac{dt(\tau)}{d\tau} = \alpha_1\alpha_1\frac{d(\ldots)}{d\not{t}},\end{aligned} \tag{48}$$

and

$$\dot{\varphi}_j = \alpha_1\overset{\circ}{\varphi}_j, \quad \ddot{\varphi}_j = \alpha_1^2\overset{\circ\circ}{\varphi}_j, \quad i=1,2,3. \tag{49}$$

In order to arrive at a more convenient setting of the system parameters, the following relation suitable for the mechanical efficiency of the engine estimation is introduced:

$$\eta_m = \frac{-L_M}{L_F}, \tag{50}$$

and on taking (46) into account, the following expression for the moment loading the engine is obtained

$$M_0 = \frac{\eta_m F_0\displaystyle\int_0^{2\pi N} p(\varphi_1)\sin\varphi_1\left(1+\frac{\cos\varphi_1}{\lambda_2\sqrt{1-\lambda_2^{-2}\sin^2\varphi_1}}\right)d\varphi_1}{2\pi N}. \tag{51}$$

Note that now the damping coefficients can be determined owing to the assumed rotational speed of the engine. Equations (40), (43), (45), (46) and (50) yield

$$c_1 = \frac{F_0(1-\eta_m)\displaystyle\int_0^{2\pi N} p(\varphi_1)\sin\varphi_1\left(1+\frac{\cos\varphi_1}{\lambda_2\sqrt{1-\lambda_2^{-2}\sin^2\varphi_1}}\right)d\varphi_1}{2\pi N((1+c_{21})+\lambda_2^{-1}(c_{21}+c_{31})(1-\sqrt{1-\lambda_2^{-2}}))\alpha_1}, \tag{52}$$

where

$$c_{21} = \frac{c_2}{c_1}, \quad c_{31} = \frac{c_3}{c_1}, \tag{53}$$

and

$$\alpha_1 = \alpha_1^{-1}\frac{\pi n}{30}. \tag{54}$$

In the above, n [rot./min.] represents the real average rotational speed of the crankshaft.

Finally, after introducing the nondimensional time $\not{t}$ and when none of the obstacles is active, the equations of motion of the piston — connecting rod — crankshaft system are as follows:

$$\mathbf{M}(\boldsymbol{\phi})\overset{\circ\circ}{\boldsymbol{\phi}} + \mathbf{N}(\boldsymbol{\phi})\overset{\circ}{\boldsymbol{\phi}}{}^{\mathbf{2}} + \mathbf{C}\overset{\circ}{\boldsymbol{\phi}} + \mathbf{p}(\boldsymbol{\phi}) = \mathbf{f}_e(\boldsymbol{\phi}), \tag{55}$$

where

$$\mathbf{C} = \alpha_1^{-1}c_1\begin{bmatrix}1+c_{21} & -c_{21} & 0\\ -c_{21} & c_{21}+c_{31} & -c_{31}\\ 0 & -c_{31} & c_{31}\end{bmatrix},$$

$$\mathbf{p}(\boldsymbol{\phi}) = -\alpha_1^{-2}\begin{Bmatrix}\sin\varphi_1\\ \mu_2\sin\varphi_2\\ \mu_3\sin\varphi_3\end{Bmatrix}, \tag{56}$$

$$\mathbf{f}_e(\boldsymbol{\phi}) = \alpha_1^{-2}\begin{Bmatrix}F_0\,p(\varphi_1)\sin\varphi_1 - M_0\\ \lambda_2 F_0\,p(\varphi_1)\sin\varphi_2\\ 0\end{Bmatrix},$$

and M_0, c_1, α_1 are determined from (51), (52), (54), respectively.

Observe that the proposed dynamical model of the piston — connecting rod — crankshaft system can be treated as a simplified model since some very important technological details are neglected. The most important simplifications are as follows: (i) tangent forces of interaction between the surfaces of the piston and the cylinder are neglected; (ii) interaction of the piston-cylinder introduced by the piston rings (by means of the friction forces

in the ring grooves in the direction perpendicular to the cylinder surface) is neglected; (iii) a simplified friction model in every joint of the system (i.e. linear damping) is assumed.

In addition, the modeling of the impact between the piston and the cylinder, where an oil layer exists, requires an approach different from the generalized restitution coefficient rule. In other words, a detailed modeling of the piston — connecting rod — crankshaft system with all essential technological details exceeds the scope of this work. However, we believe that the general model of the triple physical pendulum presented in Sec. 2 and investigated in some earlier works [Awrejcewicz *et al.*, 2001, 2002, 2003; Kudra, 2002] can serve as a good starting point for a more advanced and closer to reality dynamical model of the piston — connecting rod — crankshaft system, taking into account the lateral motion and impacts between the piston and the cylinder barrel. It should also be noticed that the presented model can govern steady state solutions of the system, and that the simulated transient motion does not correspond to the real piston — connecting rod — crankshaft system.

The dynamics of the piston — connecting rod — crankshaft system has been rigorously studied in the Habilitation Thesis [Sygniewicz, 1991]. In that monograph the following basic piston positions are assumed: (i) four piston positions in the cylinder barrel: two skew positions (with the contact between one corner of the piston and one side of the cylinder and between the opposite corner and the second side of the cylinder barrel), and two positions of the piston adjoining to one of the two sides of the cylinder surface; (ii) four displacements (turns) of the piston with one of the four corners being in contact with the cylinder.

In addition, in each of the four piston positions three equilibrium states of dynamic forces are distinguished, whereas in each of the four piston displacements two such states are distinguished. Therefore, the piston can be in one of the twenty equilibrium states of the dynamic forces. The piston movement from one side of the cylinder to the opposite side has been assumed to consist of two piston turns and one skew piston position. A direct piston movement with loss of contact with cylinder has not been analyzed.

Assuming the constant rotational speed of the crankshaft, the schedule of the forces acting on the piston and the connecting rod has been made, including tangent forces of interaction between the cylinder and the piston surfaces, forces of interaction between the piston and the cylinder via the piston rings, and assuming more real friction model in the bearings. In that way, the system of six equations of equilibrium of the dynamic forces has been obtained for the piston with the connecting rod system.

The obtained equations can be solved for one of the possible piston states for each crankshaft position. The obtained values of both normal and friction forces verify the admissibility of the assumed piston state. If the piston state is not admissible, the next piston state is assumed and the calculations are repeated until the admissible piston state is found. In that way, by varying the crankshaft position with a small angle step, for each crankshaft position one admissible piston state can be found.

Summarizing, although the model presented in [Sygniewicz, 1991] satisfies the assumed role, it does not take into account the full piston dynamics including a lateral motion of the piston in the cylinder barrel. In contrast, the full dynamical model of the piston — connecting rod — crankshaft system presented in this work, although simplified, governs the full dynamics of the piston analysis including impacts between the piston and the cylinder.

8. Numerical Examples

The nondimensional pressure distribution function $p(\varphi_1)$ used in this section and shown in Fig. 4 applies the data included in [Sygniewicz, 1991], and concerns the real pressure function obtained experimentally from the engine 1HC102 (stationary, mono-cylinder, high-pressure engine of the power of 18 KM). The period of the function is 4π ($N = 2$ for the four-stroke engine), maximal pressure $p_{\max} = 8$ MPa for the rotational crankshaft speed $n = 1200$ [rot./min.] and the full engine loading.

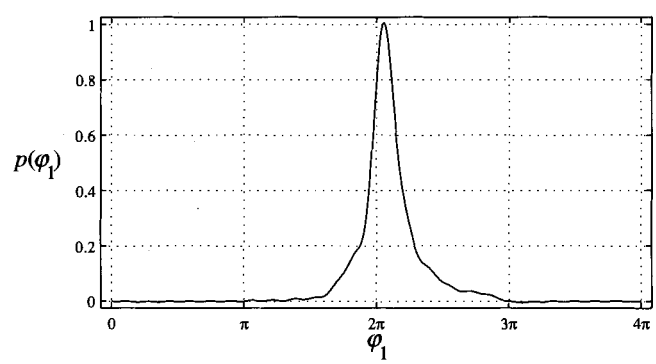

Fig. 4. Gas pressure function used for calculations.

The function $p(\varphi_1)$ is developed into the Fourier series with $K = 25$ terms. The remaining parameters are as follows: $m_1 = 10\,\mathrm{kg}$, $m_2 = 1\,\mathrm{kg}$, $m_3 = 0.4\,\mathrm{kg}$, $J_{z1} = 1\,\mathrm{kg\,m^2}$, $J_{z2} = 0.0075\,\mathrm{kg\,m^2}$, $J_{z3} = 0.001\,\mathrm{kg\,m^2}$, $l_1 = 0.04\,\mathrm{m}$, $l_2 = 0.15\,\mathrm{m}$, $e_{y1} = 0\,\mathrm{m}$, $e_{y2} = 0.12\,\mathrm{m}$, $e_{y3} = 0.01\,\mathrm{m}$, $d = 0.08\,\mathrm{m}$, $s = 0.08\,\mathrm{m}$, $h = 0.04\,\mathrm{m}$, $\eta_m = 0.85$, $c_{21} = 0.2$, $c_{31} = 0.1$, $g = 9.81\,\mathrm{ms^{-2}}$. The following real parameters are found owing to the introduced values: $\overline{M}_0 = 24.7\,\mathrm{Nm}$ and $\bar{c}_1 = 0.0288\,\mathrm{Nm^{-1}s}$. The calculations are performed for different values of the restitution coefficient and the external diameter D.

The differential equations are integrated with the time step $h_{RK4} = 2\pi/400$, and the obstacle detection accuracy is $\varepsilon_h = 10^{-12}$, the detection accuracy of the zero of the normal component of the relative velocity is $\varepsilon_{\dot{h}} = 10^{-8}$ and the detection accuracy of the zero of the normal force to the barrier surface is $\varepsilon_\lambda = 10^{-12}$ (see Fig. 1).

The initial conditions at the time instant $t = 0$ are the same for all examples: $\varphi_{10} = \varphi_{20} = \varphi_{30} = 0$, $\overset{\circ}{\varphi}_{10} = 1$, $\overset{\circ}{\varphi}_{20} = \overset{\circ}{\varphi}_{30} = 0$. In Figs. 5–10 the steady state solution is shown within the time interval $t \in (5000, 5500)$.

In order to construct some diagrams, the following nondimensional co-ordinates describing the position of the piston pin axis are used:

$$x_{O3} = \frac{\overline{x}_{O3}}{l_1} = -\sin\varphi_1 - \lambda_2 \sin\varphi_2,$$
$$y_{O3} = \frac{\overline{y}_{O3}}{l_1} = \cos\varphi_1 + \lambda_2 \cos\varphi_2. \tag{57}$$

The response of the system for the restitution coefficient $e = 0$ and the cylinder diameter $D = 0.08008\,\mathrm{m}$ (the backlash of the piston in the barrel is $0.08\,\mathrm{mm}$) is shown in Fig. 5. It is seen from the figures that the piston moves six times from one side of the cylinder to the other side during one cycle of the engine work, and most of the time the piston adjoins to one or the other side of the cylinder surface. This result confirms the well-known fact and the results presented in [Sygniewicz, 1991]. However, the piston loses contact with the cylinder while moving from one side of it to the other with a small rotation angle. This phenomenon differs from the results presented in [Sygniewicz, 1991] where it was assumed that the piston did not lose the contact with the cylinder, i.e. the piston after losing contact with the cylinder barrel at some edge, suddenly rotates until it touches the barrel on its opposite side (the rotation phase of the piston is not analyzed). But that approach does not take into account real dynamics of the piston, which is analyzed here, where the rotation phase takes a finite time interval, and impacts appear additionally. The crankshaft angular positions at the beginnings and ends of the phases of the piston adjoining and sliding along the cylinder (see the example shown in Fig. 5) differ also from the results presented in [Sygniewicz, 1991] up to 35°. The exhibited differences follow straightforwardly from the neglect of certain essential technological details in our study, as mentioned in the previous section. The most important details neglected, having most significant influence on the mentioned angles, are tangent forces of interaction between the surfaces of the piston and the cylinder and the interaction forces of the piston-cylinder introduced by the piston rings (by means of the friction forces in the ring grooves in the direction perpendicular to the cylinder surface).

In Fig. 6, the results for the larger restitution coefficient $e = 0.5$ are shown. It is seen that in general the states of the piston adjoining to the cylinder surface are the same as previously. Only the beginning of each of them is lightly delayed since the piston bounces against the cylinder a few times before the sliding occurs. Figure 7 depicts successive piston positions yielded by this solution. The results for the restitution coefficient $e = 0.9$ (Fig. 8), for the five times larger backlash between the cylinder and the piston ($D = 0.08040\,\mathrm{m}$), and for the restitution coefficient $e = 0.5$ (Fig. 9) and $e = 0.9$ (Fig. 10) are also reported. It is worth noticing that the system is at least inclined to reach the same states of the piston adjoining and sliding along the cylinder, and lasting in the same crankshaft positions as previously. Since multiple impacts between the piston and the cylinder occur, it happens that before the piston gains the motion stabilization at one cylinder side, it rapidly leaves the contact and transits into the other side of the cylinder.

It should be also noticed, that results shown in Figs. 6–10 are closer to reality since the restitution coefficient is nonzero and few impacts appear before each sliding state, but the solution shown in Fig. 5 exhibits more clearly the mentioned six stages of the piston sliding along cylinder, in particular, the ends and beginnings of each state are more distinct and easier to compare with the results in the work [Sygniewicz, 1991]. Here arises also a problem, not solved here, of proper choice of the restitution coefficient in a model, which simplifies real system, where the oil film exists between the piston and the cylinder surface.

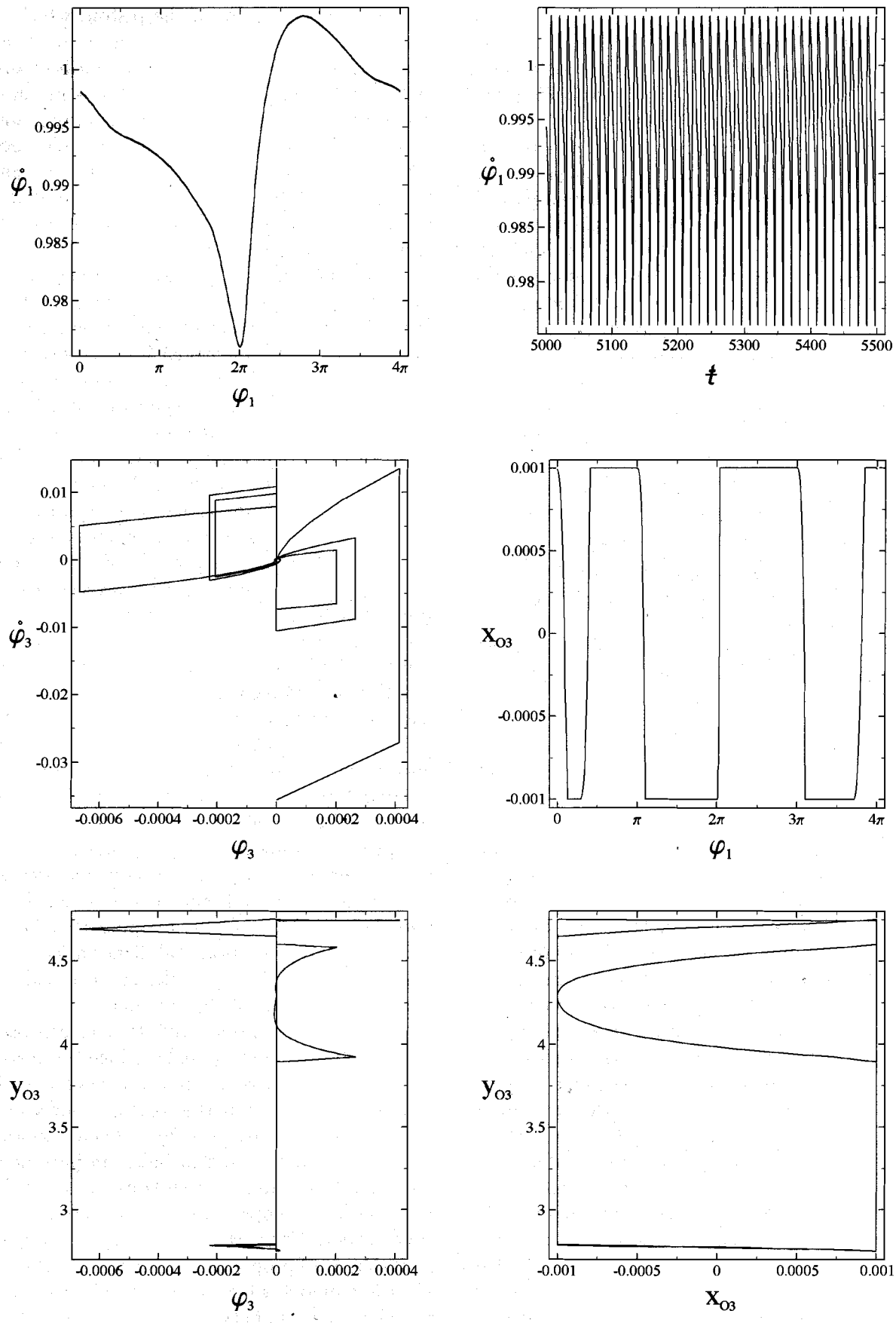

Fig. 5. System response for $e = 0$ and $D = 0.08004$ m.

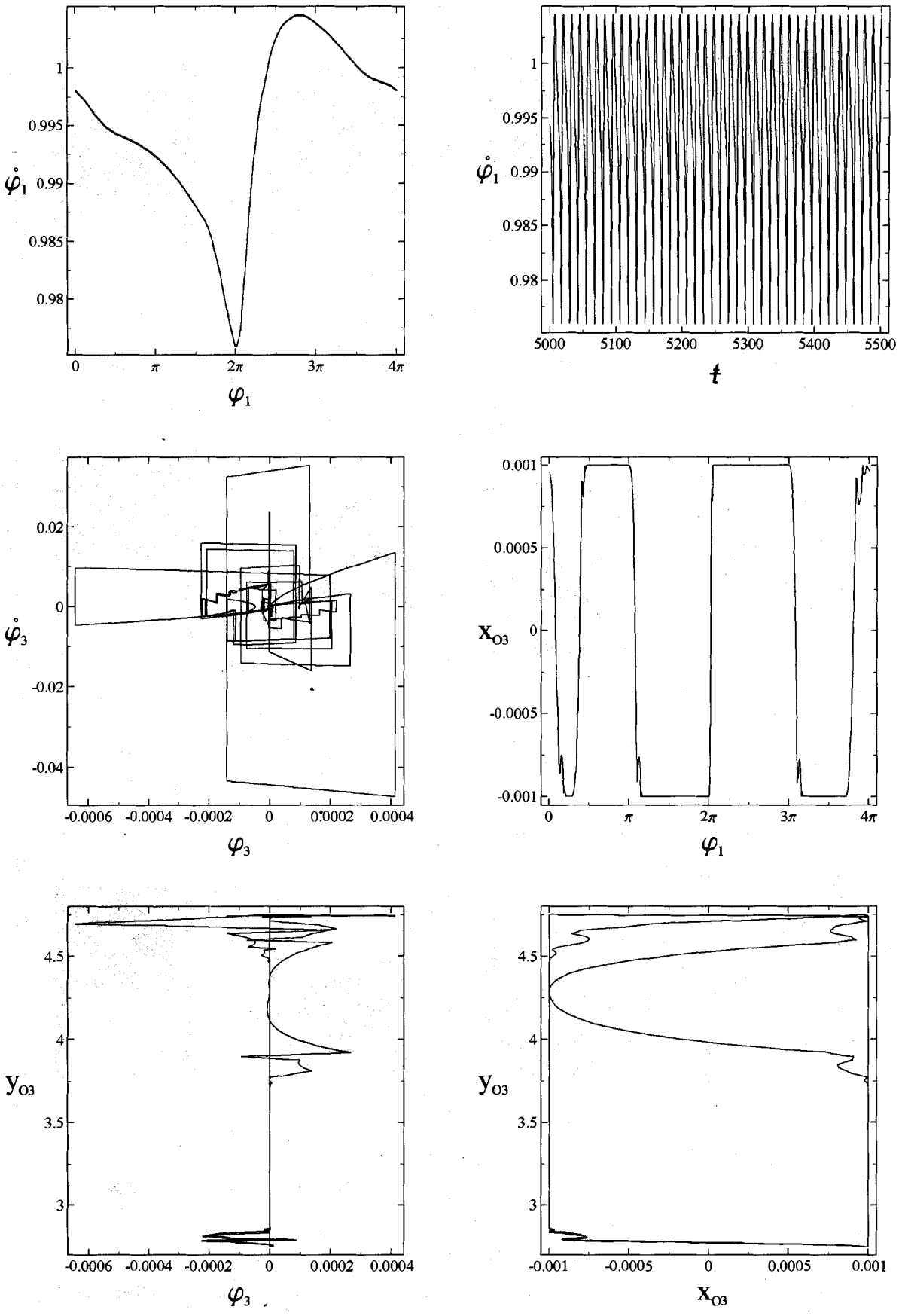

Fig. 6. System response for $e = 0.5$ and $D = 0.08008$ m.

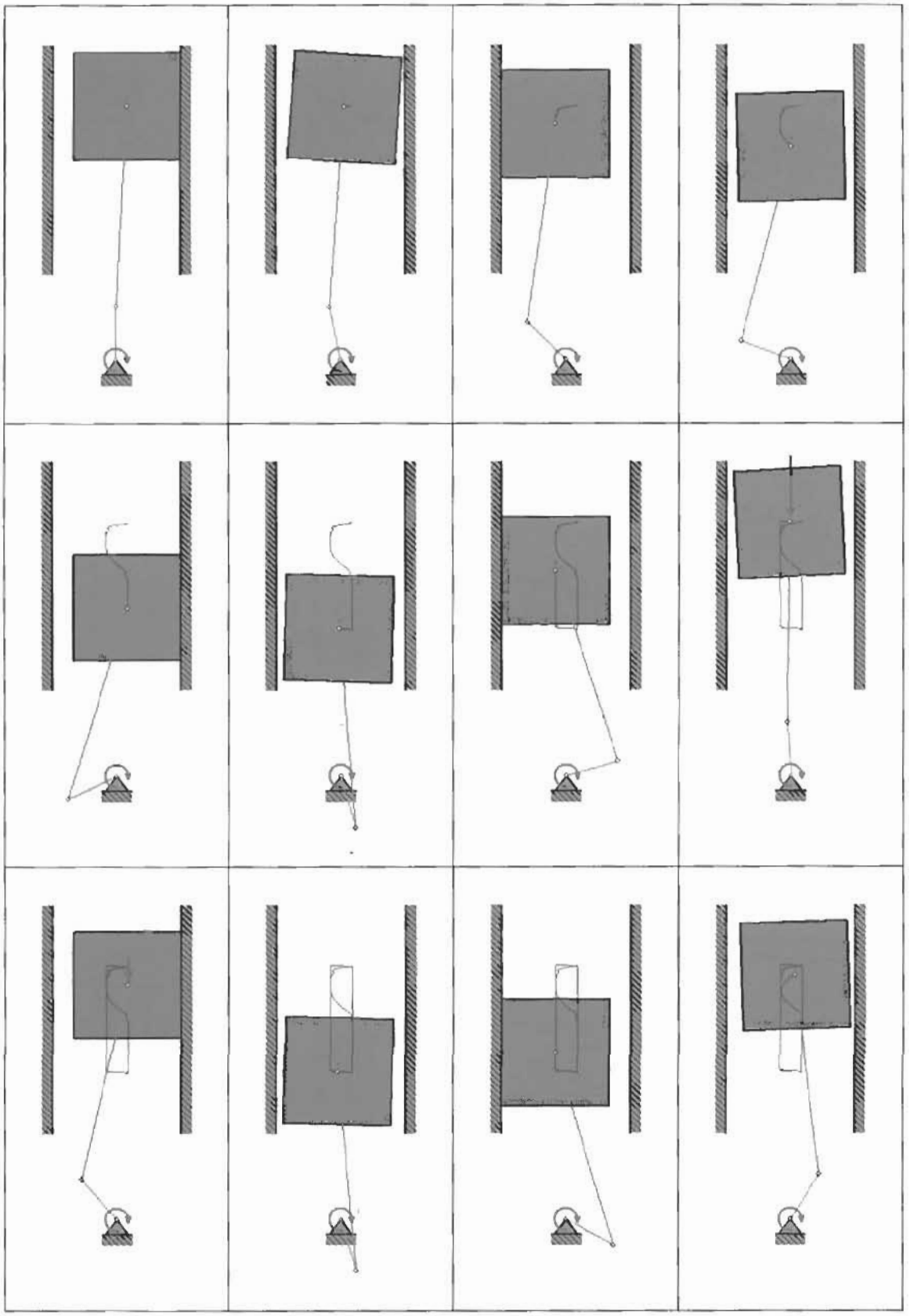

Fig. 7. Successive positions of the piston in cylindrical barrel for $e = 0.5$ and $D = 0.8008\,\mathrm{m}$.

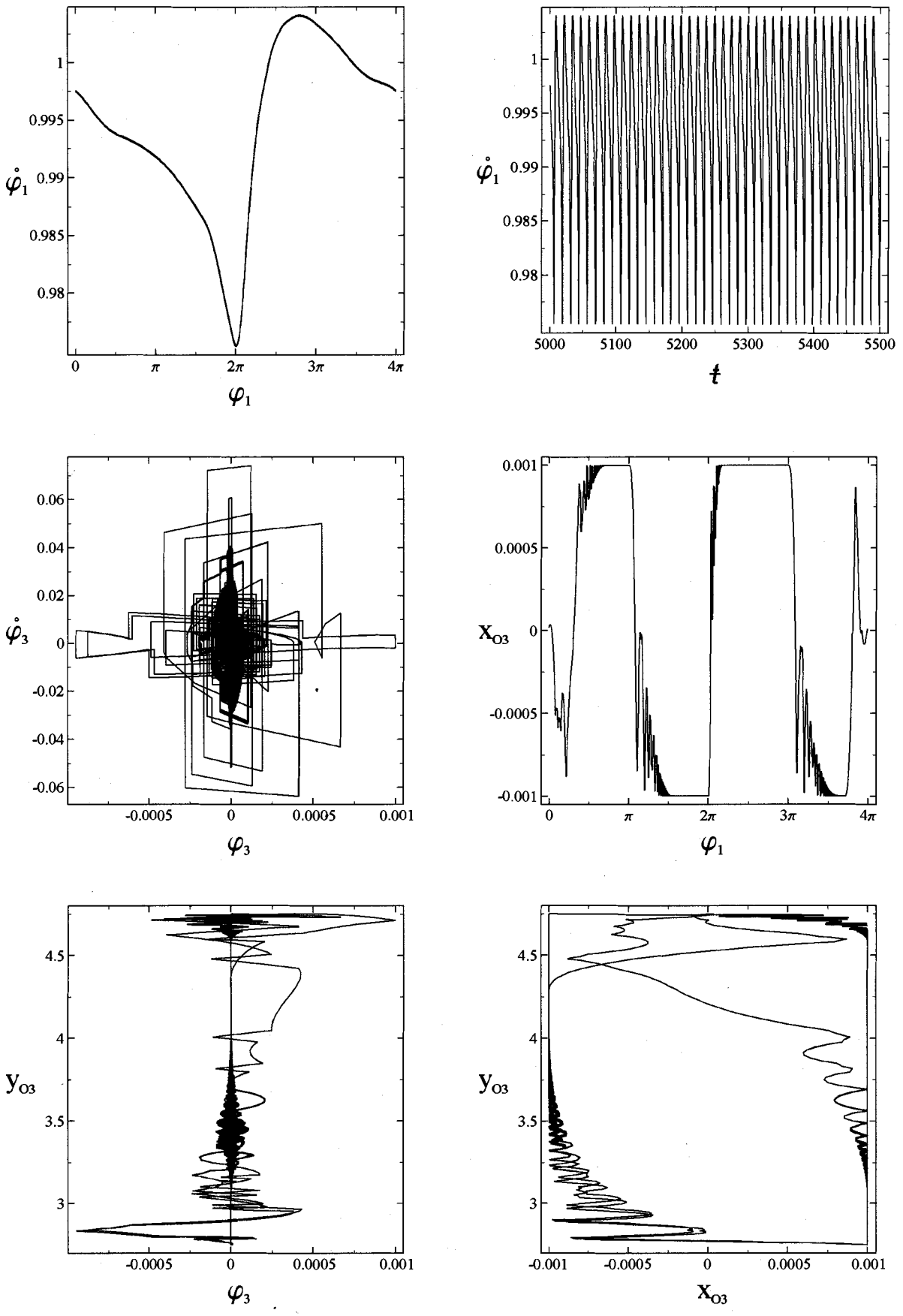

Fig. 8. System response for $e = 0.9$ and $D = 0.08008$ m.

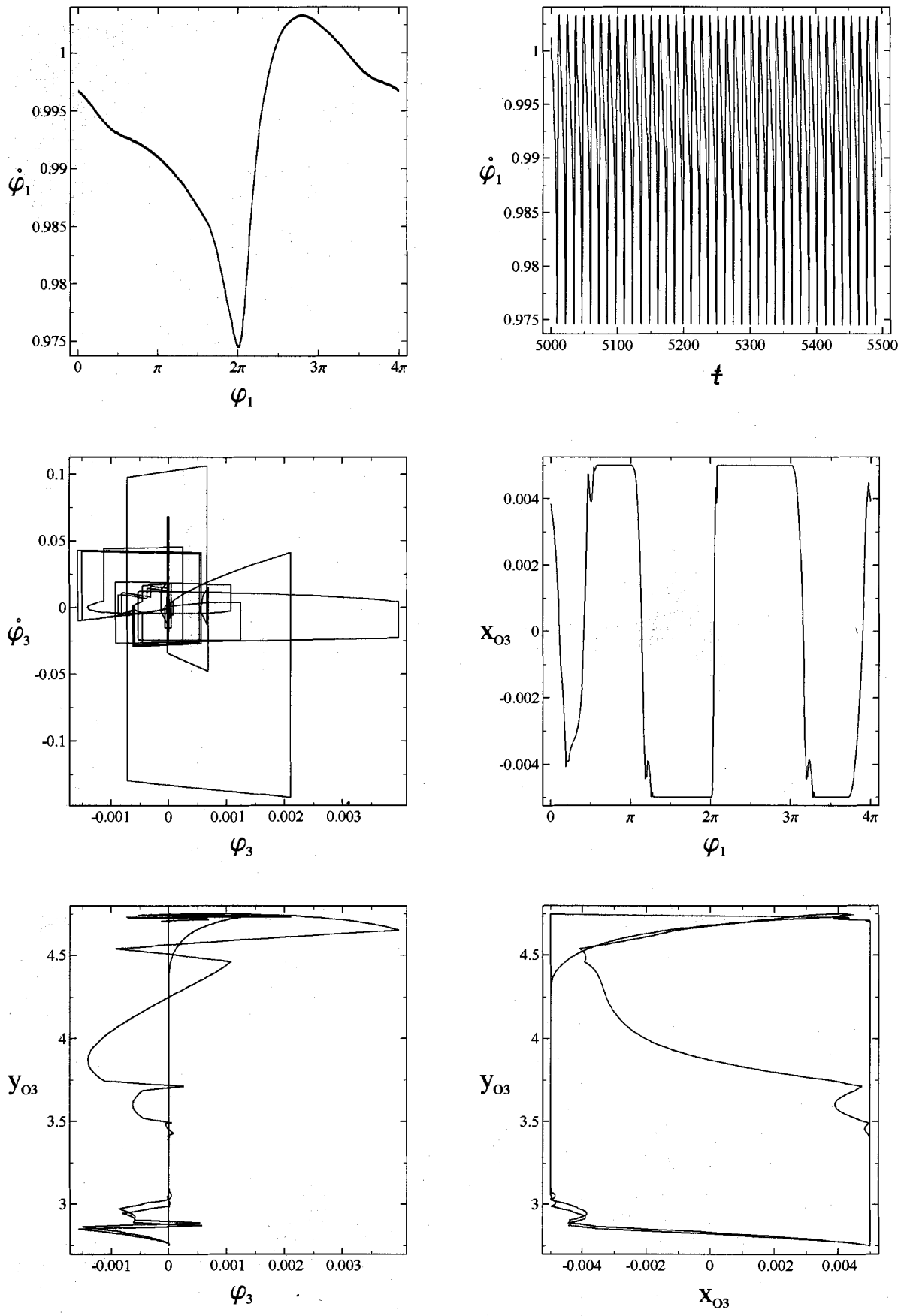

Fig. 9. System response for $e = 0.5$ and $D = 0.08040$ m.

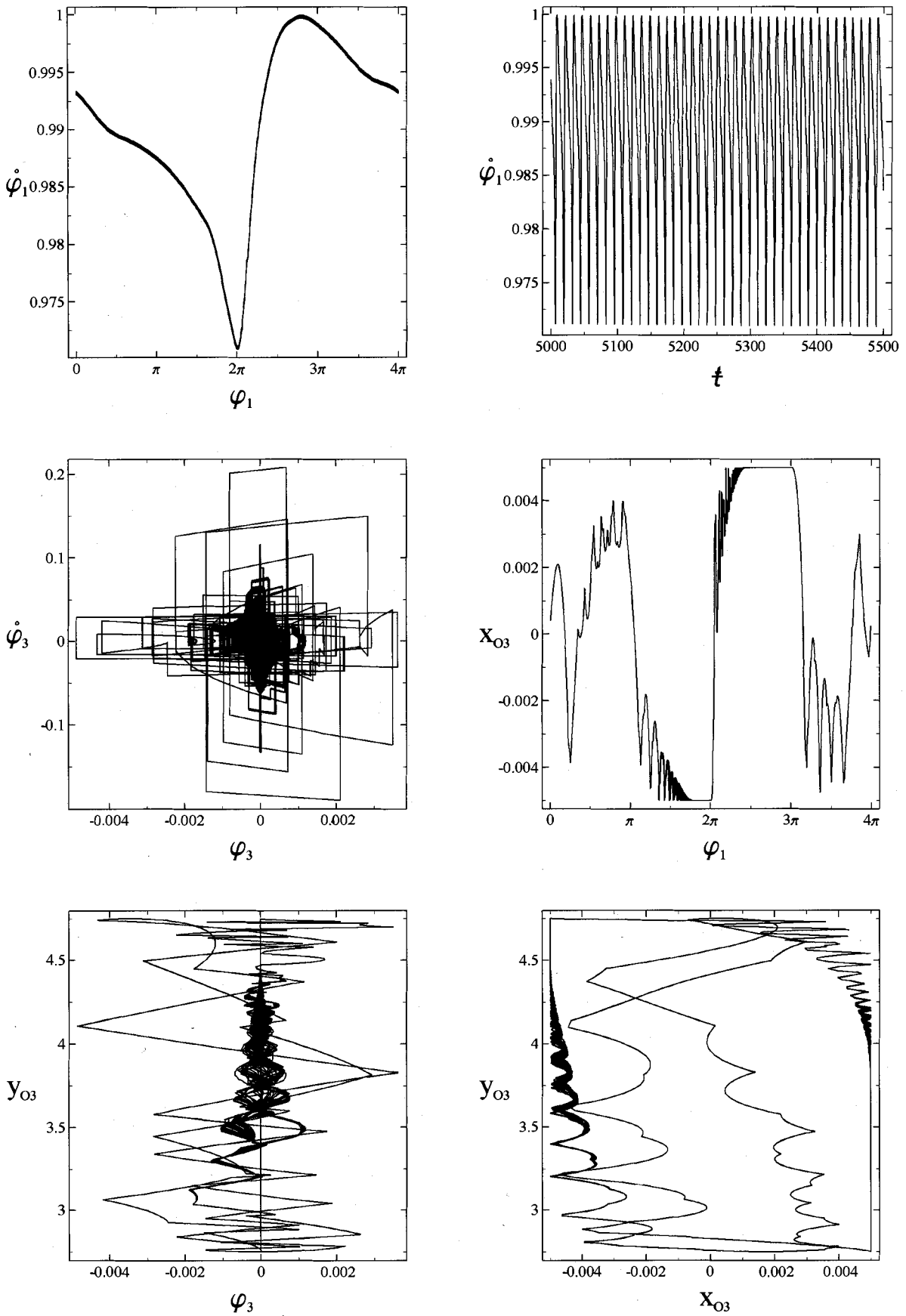

Fig. 10. System response for $e = 0.9$ and $D = 0.08040$ m.

9. Concluding Remarks

The presented solutions exhibited by the piston — connecting rod — crankshaft system modeled as a special case of the triple physical pendulum with impacts are generally similar to those described and illustrated in the monograph [Sygniewicz, 1991], although certain differences cannot be overlooked. In particular, six piston movements from one side of the cylinder to its opposite side during one cycle of the engine have been detected. Lasting states of the piston adjoining and sliding along one or the other side of the cylinder surface have mainly been observed. Some differences discussed in the previous section are due to the neglect of some essential technological details in this model. The presented model can be treated as the first step to describe the real piston-connecting rod-crankshaft system, and after taking into account certain technological details, a much better convergence with the real system behavior can be expected. Moreover, the proposed model describes the full dynamics of a piston motion in a cylinder and hence it can be very useful for the noise analysis generated by the impacts between the piston and the cylinder barrel.

Acknowledgment

The investigations presented in this work have been supported by the Polish Committee for Scientific Research (KBN) under grant No. 8 T07A 009 21.

References

Awrejcewicz, J., Kudra, G. & Lamarque, C.-H. [2001] "Analysis of bifurcations and chaos in three coupled physical pendulums with impacts," *Proc. Design Engineering Technical Conf.*, Pittsburgh, CD-ROM, 8 pp.

Awrejcewicz, J., Kudra, G. & Lamarque, C.-H. [2002] "Nonlinear dynamics of triple pendulum with impacts," *J. Techn. Phys.* **43**, 97–112.

Awrejcewicz, J., Kudra, G. & Lamarque, C.-H. [2003] "Dynamics investigation of three coupled rods with a horizontal barrier," *Meccanica* **38**, 687–698.

Ballard, P. [2000] "The dynamics of discrete mechanical systems with perfect unilateral constraints," *Arch. Rat. Mech. Anal.* **154**, 199–274.

Bishop, S. R. & Clifford, M. J. [1996] "Zones of chaotic behaviour in the parametrically excited pendulum," *J. Sound Vibr.* **189**, 142–147.

Brogliato, B. [1999] *Nonsmooth Mechanics* (Springer-Verlag, London), Chap. 6, pp. 263–282.

Kudra, G. [2002] "Analysis of bifurcation and chaos in the triple physical pendulum with impacts," PhD thesis, Technical University of Łódź, in Polish.

Pfeiffer, F. [1999] "Unilateral problems of dynamics," *Arch. Appl. Mech.* **69**, 503–527.

Strzałko, J. & Grabski, J. [1997] *Introduction to Analytical Mechanics*, Technical University of Łódź (in Polish).

Sygniewicz, J. [1991] *Modeling of Cooperation of the Piston with Piston Rings and Barrel*, Scientific Bulletin of Łódź Technical University **615/149** (in Polish).

Szemplińska-Stupnicka, W., Tyrkiel, E. & Zubrzycki, A. [2000] "The global bifurcations that lead to transient tumbling chaos in a parametrically driven pendulum," *Int. J. Bifurcation and Chaos* **10**, 2161–2175.

Szemplińska-Stupnicka, W. & Tyrkiel, E. [2002a] "Common features of the onset of structurally stable chaos in nonlinear oscillators: A phenomenological approach," *Nonlin. Dyn.* **27**, 1–25.

Szemplińska-Stupnicka, W. & Tyrkiel, E. [2002b] "The oscillation-rotation attractors in a forced pendulum and their peculiar properties," *Int. J. Bifurcation and Chaos* **12**, 159–168.

Wösle, M. & Pfeiffer, F. [1999] "Dynamics of spatial structure-varying rigid multibody systems," *Arch. Appl. Mech.* **69**, 265–285.